Trap-Limited Migration of Si Self-Interstitials at Room Temperature

K. Kyllesbech Larsen,[1,2] V. Privitera,[1] S. Coffa,[1] F. Priolo,[2] S. U. Campisano,[2] and A. Carnera[3]
[1]*CNR-IMETEM, Stradale Primosole 50, I-95121 Catania, Italy*
[2]*Dipartimento di Fisica, Università di Catania, Corso Italia 57, I-95129 Catania, Italy*
[3]*Dipartimento di Fisica, Università di Padova, Via F. Marzolo 8, I-35131 Padova, Italy*
(Received 7 August 1995)

We have investigated the room temperature diffusion and trapping phenomena of ion-generated point defects in crystalline Si. The point defects, injected by low energy Si, Ge, and Pt implants into the bulk of silicon wafers, were monitored measuring the defect-induced dopant deactivation by spreading resistance profiling. Dopant deactivation is detected up to depths of several microns beyond the region directly modified by the ions. It is demonstrated that long-range migration of Si self-interstitials is responsible for the observed phenomena.

PACS numbers: 61.72.Ji, 61.72.Tt, 66.30.Lw

The issues of defect migration, agglomeration, and interaction with substrate impurities in crystalline silicon have attracted considerable interest for both fundamental and technological reasons. In fact, the experimental determination of several properties of the vacancies (V) and self-interstitials (I), such as diffusivities and interaction cross sections, will be of invaluable importance for the description of a large variety of phenomena, such as defect evolution and damage accumulation during ion implantation, formation of secondary defects, and transient-enhanced diffusion. However, in spite of the several investigations the present knowledge of point defect diffusion and interaction in silicon is fairly poor. In fact, as a consequence of the low equilibrium concentration of point defects in crystalline silicon, any determination of their properties comes from indirect measurements and very often large discrepancies exist between different estimates of the same property. For example, defect diffusivities at high temperatures (above 800 K) are derived from the analysis of dopant, self- and metal diffusion [1–3], and from oxidation [4] and silicidation [5] experiments. The extrapolation of the derived diffusivities of vacancies and self-interstitials gives quite low room temperature diffusivities (typically less than 10^{-30} cm^2/s). On the other hand, most of the information on the structure of the defects comes from deep level transient spectroscopy (DLTS) and electron paramagnetic resonance (EPR) measurements performed at cryogenic temperatures and under electron irradiation [6,7]. From these experiments, very high room temperature diffusion coefficients of self-interstititals and vacancies are obtained [8,9] ($D_I = 3.2 \times 10^{-4}$ cm^2/s, $D_V = 4.2 \times 10^{-9}$ cm^2/s). The large discrepancy between these two sets of data has been explained by a change in the stable structure of the defects at higher temperatures, or by attributing the high diffusivity at low temperatures to ionization-enhanced migration effects induced by the electron beam.

Recent experimental investigations and theoretical calculations of the migration properties of the defects suggest that no long-range migration of point defects can occur at room temperature, and that the defect evolution during ion implantation is fully dominated by recombination and clustering inside the damaged region. Moreover, the role of C in trapping Si self-interstitials has been known for a long time [10], and its trapping properties have been recently shown [11,12] to further reduce the self-interstitial diffusivity at high temperatures (>650 °C). Molecular dynamics (MD) calculations [13] have shown that the diffusivities of the defects are quite low at least if their thermal equilibrium structure is used in the calculation. In contrast, indirect evidence of fast Si self-interstitial migration at room temperature has been recently given by Svensson, Jagadish, and Williams [14].

The aim of the present work is to give a contribution to this long-standing and controversial argument by obtaining a coherent picture of the Si self-interstitial migration at room temperature.

Experiments have been performed on *n*-type (P-doped) and *p*-type (B-doped) (100)-oriented crystalline Si wafers. In particular, epitaxial (Epi), float-zone (Fz), and Czochralski grown (Cz) Si wafers with nearly identical doping levels of $\sim 4 \times 10^{13}$/cm^3 or $\sim 3 \times 10^{15}$/cm^3 were compared. The aim is to have a large variation in the O content ($<10^{15}$/cm^3 in the Epi layers, $\sim 10^{16}$/cm^3 in Fz samples, and $\sim 10^{18}$/cm^3 in Cz samples) and in the C content of the wafers ($<10^{15}$/cm^3 in the Epi layers, $\sim 10^{17}$/cm^3 in Fz and Cz samples). These homogeneously doped substrates were implanted at 7° tilt with 40 keV Si, 90 keV Ge, and 180 keV Pt ions, to fluences ranging from 5×10^{11}/cm^2 to 5×10^{13}/cm^2, in a vacuum better than 2×10^{-7} Torr and at room temperature. The chosen energies result in a projected range of ~60 nm for all ions and in standard deviations of 33, 23, and 15 nm for Si, Ge, and Pt. The effect of the implants on the electrical activation of the dopants was studied measuring the carrier profiles by spreading resistance profiling (SRP). This technique offers the advantage of high sensitivity (1×10^{12}/cm^3) and depth resolution (better than 10 nm). The extent of the region directly modified by the ions was determined to be less than (considering

the channeling tail) 0.4 μm by secondary ion mass spectroscopy (SIMS) analyses, performed on samples implanted with 40 keV P (i.e., a mass similar to Si), 90 keV Ge, and 180 keV Pt ions.

The effect of a 40 keV $5 \times 10^{13}/\text{cm}^2$ Si implant on different homogeneously doped substrates is compared in Fig. 1. The solid lines reported in the figure result from simulations described later in the text. In Fig. 1(a) we report the carrier concentration profiles, measured by SRP analyses, of an Epi sample and of a Fz sample both P doped at a concentration of $3.7 \times 10^{13}/\text{cm}^3$. In both samples a decrease in the carrier concentration is observed in a region that, starting from the surface, extends beyond the 0.4 μm thick surface region directly affected by the ions. This result implies that in this region part of the dopants are either no longer electrically active, e.g., because they are not on a substitutional site, or that the electrically active dopants are compensated by deep levels introduced in the band gap. Both pictures involve defect migration from the ion implanted surface region into the bulk. Moreover, it should be observed in Fig. 1(a) that the extent of the modified region is much larger in an Epi than in a Fz sample. Since both samples are P doped at the same concentration level, this result suggests that the defect migration is very sensitive to the concentration of residual impurities (such as C) present in the substrate. Subtracting the 0.4 μm thick surface region, the perturbed region is $\sim$2.1 μm in epitaxial silicon and only 0.1 μm in Fz silicon. Similar results are obtained when comparing Epi and Cz silicon, as shown in Fig. 1(b) for substrates P doped at a concentration level of $\sim 3 \times 10^{15}/\text{cm}^3$. Also in this case the modified region extends deeper in the more pure Epi silicon compared to Cz silicon, which contains higher concentrations of O and C. Moreover, a comparison of the profiles measured in the Epi layers reported in Figs. 1(a) and 1(b) demonstrates that the modified depth decreases when the doping level increases. Finally, a comparison between the effect of the defect injection in the P-doped and B-doped epitaxial Si samples is provided in Fig. 1(b). Here the B-doped layer presents a more pronounced deactivation, probably because the trapping cross section of the defects is larger for B than for P.

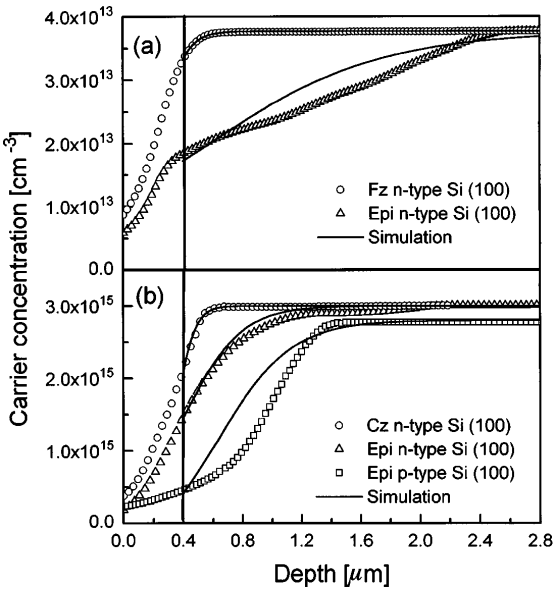

FIG. 1. SRP profiles of different homogeneously doped Si(100) substrates implanted with 40 keV ^{28}Si 5×10^{13} cm^{-2}: (a) epitaxial (Δ) and Fz ($\bigcirc$) silicon P doped at a level of 3.7×10^{13} cm^{-3}; and (b) epitaxial (Δ), Cz ($\bigcirc$) silicon P doped at 3.0×10^{15} cm^{-3}, and B-doped epitaxial Si ($\square$) with a doping level of 2.8×10^{15} cm^{-3}. The solid lines are obtained by simulations described in the text.

By integrating the measured carrier concentration profiles from a depth of 0.4 μm to the depth at which the carrier concentration level of the unperturbed substrate is reached, the areal density of dopants which have become electrically inactive, because of the Si irradiation, can be determined. The result of such an exercise, for profiles measured in *n*-type lowly doped Epi layers implanted with 40 keV Si ions at different fluences, is reported in Fig. 2. The number of deactivated atoms first increases linearly with the ion fluence and then, above a fluence of $1 \times 10^{13}/\text{cm}^2$, starts to level off. Since the residual number of active dopants has only decreased by about a factor of 2 after the implant at $5 \times 10^{13}/\text{cm}^2$, the observed saturation has to be attributed to a reduction in the injection efficiency of the defects at higher fluences.

We also compared the ability of different ions to inject defects and electrically deactivate the dopant atoms. In Fig. 3 we report the carrier concentration profiles measured on an Epi layer, P doped at a concentration of $3.0 \times 10^{15}/\text{cm}^3$, implanted with 40 keV Si, 90 keV Ge, or 180 keV Pt at a fluence of $1 \times 10^{13}/\text{cm}^2$. Although the magnitude of the deactivation increases with the ion mass, the effective length in which the deactivation is occurring is independent of the ion, confirming that it

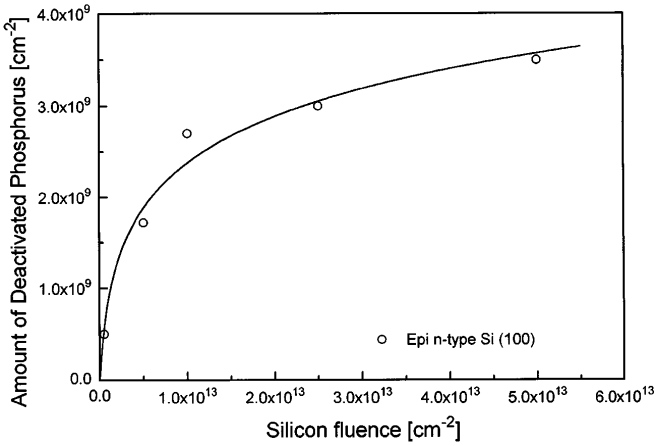

FIG. 2. Areal density of deactivated phosphorus (obtained by the integral of the concentration profile) as a function of the 40 keV Si fluence. The substrate is an epitaxial Si(100) P doped to 3.7×10^{13} cm^{-3}. The solid line is to guide the eye.

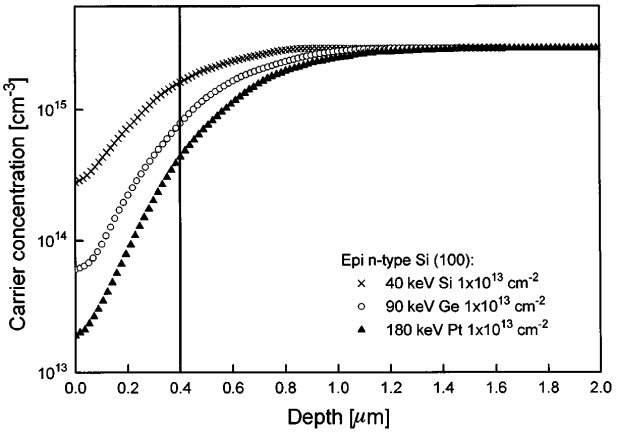

FIG. 3. SRP profiles of a homogeneously P-doped (3.0×10^{15} cm^{-3}) epitaxial Si(100) substrate implanted with (×) 40 keV Si 1×10^{13} cm^{-2}, (○) 90 keV Ge 1×10^{13} cm^{-2}, and (▲) 180 keV Pt 1×10^{13} cm^{-2}.

is determined only by the dopant and by the residual impurity concentrations. Moreover, the efficiency of injection, defined as the ratio between the number of deactivated dopant atoms and the total number of defects generated by the ion (calculated according to TRIM [15], a Monte Carlo simulation), decreases by increasing the ion mass being about 40% less for Pt than for Si ions.

The results presented so far can be interpreted inside the following scenario. Most of the defects generated by the ion beam in the surface region are either recombined or clustered into more complex defects. However, a small fraction of them can diffuse outside the implanted region and migrate into the unperturbed substrate. Here, these defects interact and can be trapped by the dopants and/or by other impurities, such as O and C. The observed dopant deactivation can result from (i) the formation of complex defects, such as divacancies, which introduce deep compensating levels in the band gap or (ii) the formation of complexes between the dopant and the defects. In order to discriminate between the different possibilities detailed simulations of the distribution, diffusion, and interaction of the point defects generated by the implants have been carried out. The Boltzmann transport equation approach [16] was used to simulate the implantation process, and a set of nonlinear coupled differential equations, describing defect annihilation and interaction, were solved numerically following the method described in Ref. [17]. We have taken into account the numerous reactions describing (i) defect recombination and clustering [i.e., formation of divacancies (V_2) and di-interstitials (I_2)]; (ii) defect interaction with dopants (i.e., formation of complexes between substitutional dopant, B or P, and I and V); (iii) interaction of defects and dopant with substrate impurities (i.e., $I + C_s \rightarrow C_i$, $V + O_i \rightarrow OV$). Among the defect complexes produced by the reactions only C interstitial (C_i) and boron interstitial (B_i) have been considered mobile at room temperature [7,18]. The parameters used in the simulation are summarized in Table I.

The simulated profiles of the active P and B atoms left after Si implantation are reported as solid lines in Figs. 1(a) and 1(b). The agreement with the experimental results is good and the model is able to explain the dependence of the spatial extent of the deactivated region on the concentration both of the dopants and of the other impurities. The calculations clearly indicate that, in spite of the fact that both I and V are injected, dopant deactivation is almost fully (>90%) determined by the interaction of the injected self-interstitials with the dopant atoms. In addition, it should be noted that V injection cannot produce the deactivation effects that we have observed in the B-doped substrates since the B-V complexes are not stable at room temperature. Also, since the injected V concentration is small, formation of divacancies is inhibited and by far overwhelmed by vacancy-impurity complexes such as OV and PV. The deep level introduced by the OV is too shallow to produce dopant compensation and the PV are known to anneal out at 150 °C. We have found that thermal annealing at temperatures up to 200 °C does not recover dopant deactivation in the highly doped n-type epitaxial silicon, demonstrating that PV are not responsible for the observed phenomena.

Having identified the interstitial injection as the main contribution to the dopant deactivation, some important information on the migration properties of the injected Si self-interstitials can be derived from the presented experimental results.

(1) The measured profiles remain stationary as a function of time. This indicates that the penetration depth of the injected Si self-interstitials is limited by the capture at trapping centers in the material. Therefore the interstitial concentration, and hence the profile of deactivated atoms,

TABLE I. Parameters used in the simulations presented in Fig. 1.

Doping level (cm^{-3})	n-type Epi 3.7×10^{13}	n-type Epi 3.0×10^{15}	p-type Epi 2.8×10^{15}	n-type Fz 3.7×10^{13}	n-type Cz 3.0×10^{15}
Impurity level					
[C] [cm^{-3}]	5.0×10^{14}	5.0×10^{14}	5.0×10^{14}	5.0×10^{16}	1.0×10^{17}
[O] [cm^{-3}]	5.0×10^{15}	5.0×10^{15}	5.0×10^{15}	2.0×10^{16}	1.0×10^{18}

Diffusivities (cm^2/s): $D_I = 3.2 \times 10^{-4}$ (Ref. [8]), $D_V = 4.2 \times 10^{-9}$ (Ref. [9]), $D_{PI} = 0.0$, $D_{PV} = 0.0$, $D_{CI} = 1.1 \times 10^{-15}$ (Ref. [18]), $D_{BI} = 3.0 \times 10^{-13}$ (Ref. [7])

decreases with a characteristic decay length given by [19] $L_I = (4\pi a_T N_T)^{1/2}$, where a_T is the trapping radius and N_T is the concentration of the traps. The results reported in Figs. 1(a) and 1(b) indicate that both dopants and other impurities, such as carbon, are efficient traps for the injected self-interstitials. Good agreement between the experimental decay length and the theoretical expression (L_I) is found. In fact, the decay length derived from the experiment is ~ 1 μm in the low-n-doped Epi silicon ($N_T < 10^{15}/\text{cm}^3$ is probably due to C), ~ 0.6 μm in the $3.0 \times 10^{15}/\text{cm}^3$ p- and n-doped Epi layers ($N_T = 3 \times 10^{15}/\text{cm}^3$ since trapping is dominated by the dopants), and <0.1 μm in Cz and Fz samples ($N_T \sim 10^{17}/\text{cm}^3$ due to C).

(2) Assuming a time of ~ 30 min for the implants and the SRP measurements, and considering that in lowly doped Epi layers the deactivation extends to 2.5 μm, it is possible to put a lower limit of 3×10^{-11} cm^2/s on the diffusion of self-interstititals at room temperature. This value is more than 20 orders of magnitude higher than that obtained by extrapolating high temperature data. Since we are considering migration occurring outside the implanted region, the large value of D_I cannot be due to ionization-enhanced mobility as in the electron irradiation experiments. The low and high temperature data can be reconciled if self-interstitials exist in at least two configurations with dramatically different mobilities.

(3) A very low fraction ($\sim 10^{-5}$) of the defects generated by the beam is injected into the substrate. Most of the generated defects do not escape recombination and clustering occurring in the implanted region. The fraction that escapes appears to be strongly dependent on the damage structure in the implanted region. In particular, the injection efficiency is reduced at high fluences, since the ions are now impinging in an already damaged region, which acts as a sink for the defects impeding their injection. The injection efficiency in also reduced for heavy ions because a large fraction of the generated defects collapses into amorphous clusters from where they cannot escape at room temperature.

We would like to thank E. Rimini for useful discussions and A. Marino, N. Parasole, and A. Spada for expert technical assistance. One of us (K. K. L.) acknowledges the financial support from the SUSTAIN network during his stay in Catania.

[1] P. M. Fahey, P. B. Griffin, and J. D. Plummer, Rev. Mod. Phys. **61**, 289 (1989), and references therein.
[2] G. B. Bronner and J. D. Plummer, J. Appl. Phys. **61**, 5286 (1987).
[3] W. Taylor, B. P. R. Marioton, T. Y. Tan, and U. Gosele, Radiat. Eff. Defects Solids **111–112**, 131 (1989).
[4] H.-J. Gossmann, C. S. Rafferty, H. S. Luftman, F. C. Unterwald, T. Boone, and J. M. Poate, Appl. Phys. Lett. **63**, 639 (1993).
[5] B. G. Svensson, M. O. Aboelfatoh, and J. L. Lindström, Phys. Rev. Lett. **66**, 3028 (1991).
[6] K. L. Brower, Phys. Rev. B **1**, 1909 (1970).
[7] G. D. Watkins, Phys. Rev. B **12**, 5824 (1975); J. R. Troxell and G. D. Watkins, *ibid.* **22**, 921 (1980).
[8] G. D. Watkins, in *Radiation Effects in Semiconductors*, edited by F. L. Vook (Plenum, New York, 1968), p. 67.
[9] S. Mottet and A. Roizés, in *Defects and Radiation Effects in Semiconductors—1978*, edited by J. H. Albany, IOP Conference Proceedings No. 46 (Institute of Physics, Bristol, 1979).
[10] G. Davies and R. C. Newman, in *Carbon in Mono-Crystalline Silicon*, Handbook of Semiconductors (North-Holland, Amsterdam, 1994), Chap. 21, pp. 1557–1636.
[11] D. J. Eaglesham, P. A. Stolk, H.-J. Gossmann, and J. M. Poate, Appl. Phys. Lett. **65**, 2305 (1994).
[12] P. A. Stolk, D. J. Eaglesham, H.-J. Gossmann, and J. M. Poate, Appl. Phys. Lett. **66**, 1370 (1995).
[13] G. H. Gilmer, T. Diaz de la Rubia, D. M. Stock, and M. Jaraiz (to be published).
[14] B. G. Svensson, C. Jagadish, and J. S. Williams, Phys. Rev. Lett. **71**, 1860 (1993).
[15] J. P. Biersack and L. H. Haggmark, Nucl. Instrum. Methods **174**, 257 (1980).
[16] L. A. Christel, J. F. Gibbons, and S. Mylroie, J. Appl. Phys. **51**, 6176 (1980); L. A. Christel and J. F. Gibbons, *ibid.* **52**, 5050 (1981); M. D. Giles and J. F. Gibbons, Nucl. Instrum. Methods **209/210**, 33 (1983).
[17] A. Hallén, D. Fenyö, B. U. R. Sundqvist, R. E. Johnson, and B. G. Svensson, J. Appl. Phys. **70**, 3025 (1991).
[18] A. K. Tipping and R. C. Newman, Semicond. Sci. Technol. **2**, 315 (1987).
[19] N. E. B. Cowern, Appl. Phys. Lett. **64**, 2646 (1994).